integration, there should be motion insensitivity to all, not just some, hyperacuity judgements.

Why is vernier acuity so little affected by movement? An important factor may be that the trajectories of the two lines do not overlap on the retina: the instantaneous positions of the two lines could therefore be compared by a mechanism that collects information over the whole extent of the motion-blurred image[8,9]. Consider, for example, a population of single units with orientationally specific receptive fields stimulated by a horizontally moving vernier target. A vertically oriented receptive field will be stimulated by the two lines of the target with a relative delay and would thus receive less stimulation than a slightly tilted field, which will be stimulated by the two lines simultaneously[9]. Although the pattern of stimulation arising from each of the moving lines is blurred, their peaks are still separately available to signal the inter-bar separation. It is not necessary that features should be discontinuous in their light distribution for the distance between them to be judged accurately, as is clear from studies of spatial-frequency discrimination using sinusoidal gratings[10].

When the two targets follow the same trajectory on the retina and when they are sufficiently close together, movement will blur them to a point where they can no longer be resolved. There is existing evidence that for separations in the region of 4 arcmin, observers base their judgments of spatial interval for static stimuli on the depth of the luminance valley between the two bars[11,12]. For example, discrimination for stimuli of this size, but not of larger separations, are severely disrupted if the two lines are of opposite luminance contrast[12]. The usefulness of the luminance-valley cue will be reduced by image motion, which will blur the two lines into a single-peaked distribution. Our subjective observations agree with this interpretation: even at low velocities the two lines comprising the 4.5-arcmin interval stimulus blurred into a single impression, in which it was difficult to see two lines.

Temporal integration would be expected to demodulate high spatial frequency components having an orientation orthogonal to the direction of motion; spatial frequency components parallel to the direction of motion will be unaffected. The high spatial frequencies in two closely spaced bars will be demodulated by motion, preventing accurate encoding of their spacing. The vernier target, on the other hand, is broad-band both in orientation and frequency, and encoding of the direction of offset does not depend exclusively on high spatial-frequency components orthogonal to the direction of motion. This explains why the interval discrimination, but not the vernier, is disrupted by motion. A simple prediction is that interval performance would not be disrupted by motion parallel to the bars and in a separate experiment we found this to be the case.

A further prediction is that spatial interval acuity will be less adversely affected by image motion if the standard separation between the bars is increased. Increasing the separation will mean that the two bars are increasingly resolved, despite being spread out by motion blurring. We tested this prediction by using standard intervals of 9, 18 and 36 arcmin. The observers were the two of us and two other naive observers. Our results confirm the prediction (Fig. 2). The more widely separated targets are less susceptible to motion. Indeed, thresholds for the 36-arcmin separation show a degree of motion insensitivity comparable to that for vernier acuity. Analysis of variance of these data confirmed the predicted interaction between stimulus velocity and standard interval size ($F = 3.76$; d.f. $= 8.24$; $P < 0.0056$).

There have been previous reports of constraints on the ability of the visual system to deal with moving targets[7,13]. If there is a general deblurring mechanism in human vision, it would maintain resolution of even closely spaced lines. The fact that it does not do so leads us to conclude that the striking insensitivity of vernier acuity to motion depends not on the removal of motion blur, but on the fact that motion blur does not degrade the critical information in the stimulus. □

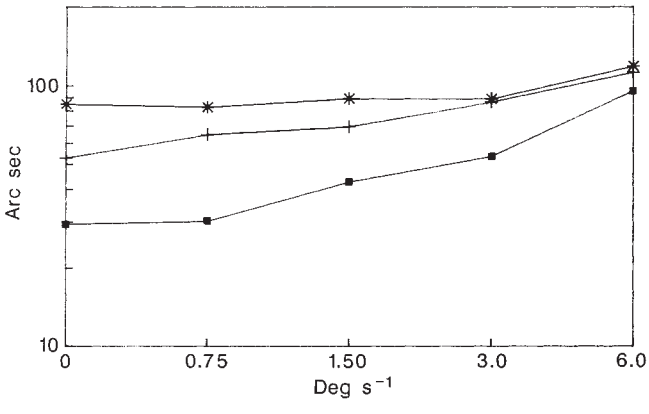

FIG. 2 Thresholds for spatial-interval acuity determined for three standard intervals: 9 arcmin, small square; 18 arcmin, cross; 36 arcmin, star. Results support the prediction that motion would have less of an effect at wider standard intervals. The data points are means for four different observers (M.M., S.B., R.C. and G.H.). The experimental methods were the same as in Fig. 1 except for masking of the ends of the target trajectories. On every trial, each of the target bars was randomly and independently switched off either 0, 4 or 8 arcmin before the end of its trajectory.

Received 7 April; accepted 16 June 1989.

1. Burr, D. C. *Nature* **284,** 164–165 (1980).
2. Burr, D. C., Ross, J. & Morrone, M. C. *Proc. R. Soc.* B**227,** 249–265 (1986).
3. Anderson, C. H. & Van Essen, D. C. *Proc. natn. Acad. Sci. U.S.A.* **84,** 6297–6301 (1987).
4. Westheimer, G. & McKee, S. P. *J. opt. Soc. Am.* A**65,** 847–850 (1975).
5. Westheimer, G. & McKee, S. P. *Vis. Res.* **17,** 941–947 (1977).
6. Westheimer, G. H. *Am. med. Ass. Archs Ophthal.* **52,** 932–941 (1954).
7. Morgan, M. J., Watt, R. J. & McKee, S. P. *Vis. Res.* **23,** 541–546 (1983).
8. Morgan, M. J. *Phil. Trans. R. Soc.* B**290,** 117–135 (1980a).
9. Morgan, M. J. & Watt, R. J. *Vis. Res.* **23,** 997–1003 (1983a).
10. Campbell, F., Nachmias, J. & Jukes, J. *J. opt. Soc. Am.* A**60,** 555–559 (1970).
11. Klein, S. A. & Levi, D. M. *J. opt. Soc. Am.* A**2,** 1170–1190 (1985).
12. Levi, D. M. & Westheimer, G. *J. opt. Soc. Am.* A**4,** 1304–1313 (1987).
13. Welch, L. & McKee, S. P. *Vis. Res.* **25,** 1901–1910 (1985).

ACKNOWLEDGEMENTS. This work was supported by the Medical Research Council.

The colour centre in the cerebral cortex of man

C. J. Lueck*†‡, S. Zeki†§, K. J. Friston*, M.-P. Deiber*, P. Cope†, V. J. Cunningham*, A. A. Lammertsma*, C. Kennard‡ & R. S. J. Frackowiak*§

* MRC Cyclotron Unit, Hammersmith Hospital, DuCane Road, London W12 0HS, UK
† Department of Anatomy, University College London, Gower Street, London WC1E 6BT, UK
‡ Department of Neurology, The London Hospital, Whitechapel, London E1 1BB, UK

ANATOMICAL and physiological studies have shown that there is an area specialized for the processing of colour (area V4) in the prestriate cortex of macaque monkey brain[1]. Earlier this century, suggestive clinical evidence for a colour centre in the brain of man[2,3] was dismissed[4–8] because of the association of other visual defects with the defects in colour vision[4,5,7]. However, since the demonstration of functional specialization in the macaque cortex[9], the question of a colour centre in man has been reinvestigated,

§ To whom reprint requests should be addressed.

based on patients with similar lesions in the visual cortex[10–12]. In order to study the colour centre in normal human subjects, we used the technique of positron emission tomography (PET), which measures increases in blood flow resulting from increased activity in the cerebral cortex. A comparison of the results of PET scans of subjects viewing multi-coloured and black-and-white displays has identified a region of normal human cerebral cortex specialized for colour vision.

The increases in blood flow resulting from increased activity in the cerebral cortex can be measured using PET. Our aim was to detect colour-processing areas of the cerebral cortex by presenting normal human subjects with visual stimuli highlighted for colour, and looking for regions of increased activity using PET. Because most stimuli are likely to activate several specialized visual areas, such as those concerned with motion and form, we used an abstract display of coloured squares and rectangles (a 'Mondrian')[13] to maximize stimulation of areas responsive to colour and minimize the activation of other cortical areas. This display was used on experimental trials (colour trials). For control trials (grey trials) we used a display that was identical, except that the rectangles were of different shades of grey, each grey isoluminant with its coloured counterpart. Isoluminant grey values were determined by converting the relevant colour and its corresponding grey into an alternating moving grating. The luminance of the grey grating was adjusted until the perception of motion ceased[14]. We expected that, when compared with the resting (eyes closed) state, activity would be greatly enhanced by the colour stimulus in areas V1 and V2, both of which have compartmentalized groups of wavelength-selective cells[15–17], as well as in the human homologue of V4. The grey display would produce such enhancement only in V1 and V2. As the emission from each grey rectangle included light from all phosphors, the wavelength-selective cells in V1 and V2 were expected to respond to their preferred wavelengths[18].

A PET-scanner (ECAT 931/8/12) (CTI Inc., Knoxville) with an intrinsic spatial resolution of $5.5 \times 5.5 \times 7.0$ mm full-width at half-maximum (FWHM)[19] allowed the simultaneous collection of 15 contiguous transaxial planes, giving a total axial field of view of 10.5 cm. The set of scans was collected so that the lower border of the first transaxial slice was on the orbito-meatal line. Scans were reconstructed using a Hanning filter with a cut-off frequency of 0.5 cycles per pixel, producing a parametric image of cerebral blood flow, with a resolution of $8.5 \times 8.5 \times 7.0$ mm[19]. The set of data was then expanded by bilinear interpolation in the axial (z) dimension to produce 43 transaxial slices. This enabled the data to be displayed in a $128 \times 128 \times 43$ voxel matrix, each voxel having similar dimensions in each of the three axes.

Cerebral blood flow was measured using an integral/dynamic technique[20]. Subjects inhaled trace amounts of $C^{15}O_2$ for 2 min. Dynamic scans, starting 0.5 min before gas administration, were as follows: 1×30 s, 4×5 s, 16×10 s. The scanning sequence therefore spanned brain build-up and wash-out phases of the flow tracer ($H_2{}^{15}O$ is produced by the transfer of ^{15}O from $C^{15}O_2$ in the lung capillaries[21,22]). The first 30-s frame was used to correct for residual background activity from previous scans. Throughout scanning, arterial radioactivity was sampled every second by an on-line beta ($\beta+$)-probe. Blood was continuously withdrawn through a small radial-artery cannula at a rate of 5 ml per min. Delay and dispersion of the arterial time-activity curves in the radial artery, cannula and external tubing were measured using a method described previously[23]. The corrected arterial input functions were then used to calculate regional cerebral blood flow (rCBF) on a pixel-by-pixel basis, using an integral method applied to the 2-min build-up phase[20]. Radioactivity distributions were thus transformed into quantitative parametric images of cerebral blood flow.

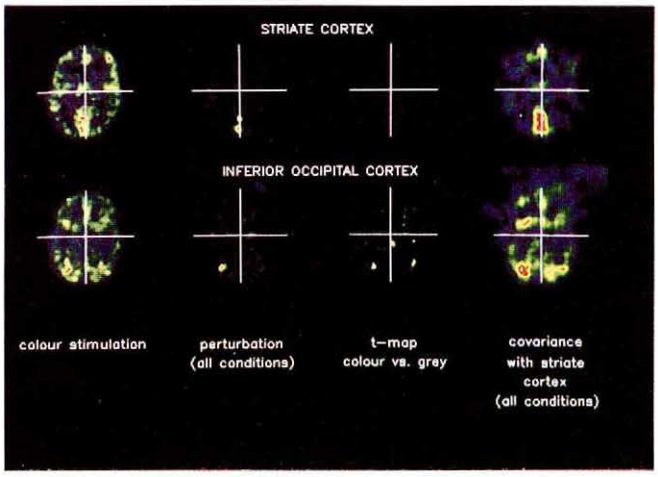

FIG. 1 Parametric and statistical scans at the level of striate and inferior occipital cortices. Colour stimulation: parametric images of rCBF. The striate cortex is 1.2 cm above the AC-PC line and the inferior-occipital cortex 1.7 cm below it. Perturbation: map perturbation (variance) calculated from the pixel-by-pixel grey-value variance across all six scans divided by the difference in grey values between the two rest scans (a reflection of noise). To reduce noise, each scan was smoothed using a low-pass filter of side length 5 pixels (10.25 mm). t-Map: t-statistic map showing the significance of any difference between colour- and grey-activated scans. To remove variance resulting from changes in global blood flow, the original scans were normalized to a total brain blood flow of 50 ml 100 ml^{-1} min^{-1}. As the study aimed to locate an area maximally responsive to colour but not grey, a one-tailed t-test was used. Covariance map: the covariance of grey values for all six scans with the grey values of a reference pixel located in the striate cortex. White and red represent the greatest activity/significance/covariance, and blue the least.

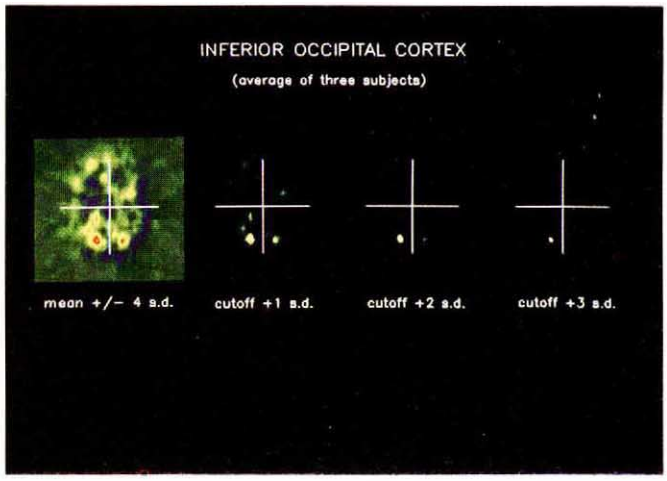

FIG. 2 Standardized difference between colour- and grey-activation scans for inter-subject averaged data. In generating the left-hand scan, the normalized, averaged scans for the stimuli from each subject have been re-sized into a standard-proportional format, permitting pixel-by-pixel inter-subject averaging. The mean grey data were subtracted from the mean colour data after filtering with a 9×9 pixel (18.45×18.45 mm) matrix. This filter was used for inter-subject analysis because of additional variance introduced by normal anatomical variability. The data are in terms of the grey-value difference between conditions (red indicates increased activity during colour stimulation, blue increased activity during grey, and green ~ equivalent activity). Subsequent images have thresholds at 1, 2 and 3 s.d. above the mean, respectively. Plane of section is 6 mm below the AC-PC line.

(a)

Absolute cerebral blood flows (ml 100 ml^{-1} min^{-1} to nearest ml)

	Large regions of interest					
	Left			Right		
	Rest	Colour	Grey	Rest	Colour	Grey
Striate	54	64	58	—	—	—
Cortex	51	60	58	—	—	—
(midline)	54	60	58	—	—	—
Mean	**53**	**61**	**58**	—	—	—
'Colour	53	57	47	51	57	47
area'	50	60	55	55	60	57
	37	44	36	37	45	39
Mean	**47**	**54**	**46**	**48**	**54**	**48**
Temp.-occ.-	42	42	38	44	45	41
parietal	42	52	49	44	51	50
pit	41	39	37	40	37	36
Mean	**42**	**44**	**41**	**42**	**45**	**42**
Frontal	44	46	41	44	46	43
eye fields	50	50	50	55	57	58
	46	41	41	48	44	43
Mean	**47**	**46**	**44**	**49**	**49**	**48**
Primary	47	47	44	49	48	47
motor	51	52	50	47	48	49
cortex	52	51	49	54	50	48
Mean	**50**	**50**	**48**	**50**	**49**	**48**
	Small region of interest					
'Colour	50	76	58	45	55	40
area'	38	55	44	48	56	55
	35	44	36	37	47	43
Mean	**41**	**58**	**46**	**44**	**53**	**46**

(b)

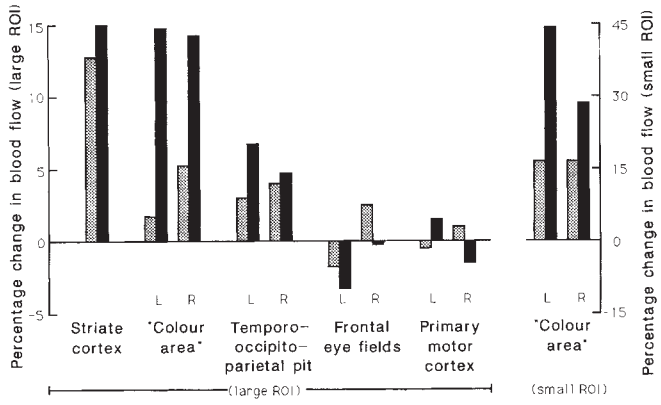

FIG. 3 rCBF and percentage change in rCBF in different regions of the brain. Results are based on absolute cerebral blood flow (*a*) or on normalized data (*b*). In *b*, changes in both colour (black) and grey (stippled) stimulated states are shown as percentage increases over the resting state. The large region of interest (ROI) comprises 180 pixels—1.8 cm in diameter and 0.6 cm in height. Its size is based on the s.d. of the separation of colour areas between different subjects (Table 1). The large ROIs were centred in individual's scans on co-ordinates defined by the region of greatest change observed on the inter-subject averaged, grey-colour difference scan (Fig. 2). Other areas include the striate cortex, frontal eye fields, and primary motor cortex. Also shown are the rCBF and percentage changes in a region around the temporo-occipito-parietal pit, possibly the human homologue of area V5. To assess the maximum change in activity across subjects, a small ROI of 16 pixels (diameter corresponding to the FWHM) was positioned around the areas of maximal colour-induced activity in each subject. L, left; R, right.

Scans were analysed on a computer (SUN 3/60) with image-analysis software (ANALYZE; BRU, Mayo Clinic), which allowed scans to be scaled to standard stereotactic co-ordinates based on the Talairach atlas[24] and to be displayed relative to the intercommissural line (AC-PC line). This permitted anatomical localization[25] and averaging of data across different subjects.

Three normal male volunteers, of whom two were left-handed, were presented stimuli displayed on a high-resolution colour-television monitor occupying the central 40° of the visual field, corresponding to that represented in V4 (ref. 2). All extraneous light was excluded and other sources of sensory stimulation minimized. To avoid visual fading, subjects moved their eyes to track backwards and forwards along a line (subtending 5°) in the centre of the display. Each subject underwent six scans. Scans 1 and 6 were rest (eyes shut); 2 and 5 were colour trials; and 3 and 4 were grey trials. Each scan lasted 3.5 min, and 15 min separated scans to allow for isotope decay (the half life of ^{15}O is 2.1 min). Head movement between scans was prevented by the use of head holders of expanded polystyrene.

We analysed our results using statistical methods developed for use with small numbers of subjects. The perturbation studies and covariance maps (Fig. 1) were primarily aimed at finding cerebral areas showing altered activity with visual stimuli and which covaried with activity in the striate cortex. For all subjects, the area of the lingual and fusiform gyri in the inferior occipital region was highlighted by both techniques (Fig. 1).

A pixel-by-pixel map of the *t*-value for the difference between the average of the two colour scans and the average of the two grey scans was constructed for each subject (*t*-map; Fig. 1). The value of the *t*-statistic made the null hypothesis highly unlikely, suggesting that the perturbed areas in the lingual and fusiform gyri were specifically involved in colour processing ($P \leq 0.05$). This was further confirmed by change-distribution analysis of data averaged across individuals (Fig. 2). The precise anatomical locations of the activated areas within these gyri varied between the individual subjects, reflecting anatomical variability (Table 1).

As expected, there was minimal difference in activity in the striate cortex in response to grey or colour stimulation. We suppose that the area adjoining the striate cortex, area V2, was similarly active in both conditions, but the resolution of the scanner was not fine enough to distinguish the two areas. The only area surrounding the striate cortex consistently showing a significant increase in activity during colour but not during grey stimulation was located in the region of the lingual and fusiform gyri, in agreement with earlier clinical suggestions[2]. We refer to this as the 'colour area', although the determination of colour may not be its only function. We presume this area is the homologue of area V4 in the macaque monkey.

To obtain quantitative data, the activity was sampled from regions of interest defined on the rCBF scans (Fig. 3). In the

TABLE 1 Anatomical location of 'colour areas'

Subject	Side	*x* (mm)	*y* (mm)	*z* (mm)	Distance from mean (mm)
Mean of three	Right	+24	−58	−7	—
	Left	−27	−56	−5	—
Individual brains:					
1	Right	+46	−49	−17	25
	Left	−41	−57	−17	19
2	Right	+10	−49	+5	21
	Left	−24	−56	+3	8
3	Right	+20	−61	−8	5
	Left	−30	−61	−6	6

Distances to nearest mm; reference midpoint of AC-PC line.

striate cortex there was an increase in activity (13–15%) over the resting state for both colour and grey trials (normalized data). An increase of 12–14% was seen in the colour areas during colour but not grey stimulation. There was a 3–5% increase in activity in the region of the temporo-occipito-parietal pit (thought to correspond to area V5 involved in the analysis of visual motion[26,27]) for both colour and grey trials. Activity in the frontal eye fields and primary motor cortex was little affected by visual stimulation. For normalized data, the average increase in flow in a smaller region of interest centred on the colour area during colour stimulation compared with that during grey was 28% on the left hemisphere and 12% on the right, percentages being those of baseline (rest) flow.

Because of the small increase in flow in V5 seen in our trials, we tested a fourth subject and compared the areas activated by colour simulation with those activated by a stimulus of black random dots ($1° \times 1°$) moving against a white background at 6° per s, with the direction of motion changing every 15 s. In this subject, an area on the lateral surface of the occipito-temporal boundary, corresponding in position to the human homologue of V5 (ref. 27), showed significantly increased activity during motion presentation. Also, a zone in the colour area showed significant increase during colour but not motion stimulation. This suggests that the increase in activity in the homologue of V5 seen in our initial subjects may have been due to other factors, such as movement of the visual image on the retina generated by eye movements during stimulation.

There were two unexpected results. First, the activity in the colour area of the left hemisphere was greater than that of the right, regardless of whether the subject was left-handed. We are unable to explain this; there is no published suggestion of hemispheric dominance in the analysis of colour. Second, there was no substantial change in activity in the temporal cortex, to which V4 projects in the macaque monkey[28]. This suggests that the colour area is sufficient for the determination of colour when there is no involvement of memory or experience, an idea requiring further study. In summary, by using modern technology we have been able to demonstrate the existence of a specialized colour centre in the brain of normal man for the first time. □

Received 13 March, accepted 23 June 1989.

1. Zeki, S. M. *Brain Res.* **53,** 422–427 (1973).
2. Verrey, *Archs Ophthalmol., Paris* **8,** 289–300 (1888).
3. MacKay, C. & Dunlop, J. C. *Scottish med. Surg. J.* **5,** 503–512 (1899).
4. Henschen, S. C. in *Handbuch der Neurologie, 2* (ed. Lewandowsky, M.) 891–918. (Springer, Berlin, 1910).
5. von Monakow, C. *Gehirnpathologie* Vol. IV (Hölder, Vienna, 1905).
6. Holmes, G. *Proc. R. Soc.* **B 132,** 348–361 (1945).
7. Monbrun, A. *Traité d'ophthalmologie* (Societé Française d'ophthalmologie, Masson & Cie., Paris, 1939).
8. Duke-Elder, J. *A System of Ophthalmology* Vol. V (Churchill, London, 1971).
9. Zeki, S. M. *Nature* **274,** 423–428 (1978).
10. Pearlman, A. L., Birch, J. & Meadows, J. C. *Ann. Neurol.* **5,** 253–261 (1979).
11. Damasio, A., Yamada, T., Damasio, H., Corbett, J. & McKee, J. *Neurology* **30,** 1064–1071 (1980).
12. Kölmel, H. W. *Eur. Arch. psychiatr. Neurol. Sci.* **237,** 237–243 (1988).
13. Land, E. H. *Proc. R. Inst. Gt Br.* **47,** 23–57 (1974).
14. Anstis, S. & Cavanagh, P. in *Colour Vision. Physiology and Psychophysics* (ed. Mollon, J. D. & Sharpe, L. T.) 155–166 (Academic, London, 1983).
15. Shipp, S. & Zeki, S. *Nature* **315,** 322–325 (1985).
16. DeYoe, E. A. & van Essen, D. C. *Nature* **317,** 58–61 (1985).
17. Hubel, D. H. & Livingstone, M. S. *J. Neurosci.* **7,** 3378–3415 (1987).
18. Zeki, S. *Neuroscience* **9,** 741–765 (1983).
19. Spinks, T. J., Jones, T., Gilardi, M. C. & Heather, J. D. *IEEE Trans. nuc. Med.* **35,** 721–725 (1988).
20. Lammertsma, A. A. *et al. J. Cereb. Blood Flow Metabol.* (suppl.) (in the press).
21. West, J. B. & Dollery, C. T. *J. appl. Physiol.* **17,** 9–13 (1962).
22. Frackowiak, R. S. J., Lenzi, G. L., Jones, T. & Heather, J. D. *J. Comput. Assist. Tomogr.* **4,** 727–736 (1980).
23. Lammertsma, A. A. *et al. J. Cereb. Blood Flow Metabol.*, in the press.
24. Talairach, J. *et al. Atlas d'Anatomie Stéréotaxique du Téléncephale* (Masson & Cie, Paris, 1967).
25. Friston, K. J. *et al. J. Cereb. Blood Flow Metabol.* (in the press).
26. Zeki, S. M. *J. Physiol., Lond.* **236,** 549–573 (1974).
27. Mora, B. & Allman, J. M. *Trends Neurosci.* (in the press).
28. Desimone, R., Fleming, J. & Gross, C. G. *Brain Res.* **184,** 41–55 (1980).

ACKNOWLEDGEMENTS. We thank Miss C. Taylor for her help in scanning the patients, R. Robb (Mayo clinic) for the use of the ANALYZE software package, our colleagues in the MRC Cyclotron Unit Chemistry and PET Physics Sections, and the Wellcome Trust for their help and support. In addition we thank J. Romaya for providing the program for the motion stimulus.

Ageing and mutation in plants

Edward J. Klekowski Jr & Paul J. Godfrey

Botany Department, University of Massachusetts, Amherst, Massachusetts 01003, USA

PLANTS have many characteristics allowing the accumulation of somatic mutations: lack of a germ line, open systems of growth, flexible meristem organizations and the fact that most somatic mutations are not immediately life-threatening.[1]. A consequence of this is that the meristematic initials of a plant accumulate mutations as it ages[2–4]. We report here that the mutation rates in the long-lived mangrove are 25 times higher than in the annuals barley and buckwheat. An increase in the frequency of mutant initials is, in effect, an increase in the mutation rate per generation, leading to the prediction that long-lived plants will have higher mutation rates per generation than short-lived plants. Because the mutation rate per generation is the primary determinant of inbreeding depression and the dominant and recessive components of genetic load[5–7], plant age and/or life span[8] may be a critical and generally unrecognized aspect of the evolutionary equation.

Estimates of forward mutation frequencies and rates are very rare in long-lived plants[9]. Perhaps the easiest mutant phenotype to detect in higher plants is chlorophyll deficiency or albinism. Based on mutagen studies in barley, the number of nuclear gene loci that can mutate and result in a chlorophyll-deficient phenotype is ~300 (refs 10,11). Thus, this mutant phenotype has a mutation rate that is the sum of the individual mutation rates for each of these loci. Because the genetic organization of the photosynthetic process is ancient and highly conserved, it is likely that a similar number of nuclear gene loci occurs in most angiosperms.

Rhizophora mangle is a diploid ($2n = 36$) woody tree that can reach 25 m in height. The species is unable to reproduce vegetatively, although individual specimens can be widespread because of the support given to lateral branches by 'prop roots' (ref. 12). A peculiar habit of *R. mangle*, as well as other mangrove species, is vivipary, the germination of the seed while still on the tree[13,14]. The floral biology of *Rhizophora* is characterized by hermaphroditic flowers, anthers dehiscent in the floral bud, and a short functional life of the flower. Primack and Tomlinson[15] hypothesized that mangrove species are self-compatible and more highly inbred than other tropical woody plants. Our results provide strong support for their hypothesis.

Because of self-compatibility and vivipary, *R. mangle* is an ideal organism for mutation studies. The prolonged development of the chlorophyll-containing embryo hypocotyl allows detection of albino embryos while they are attached to the parental tree (Fig. 1). Thus parent and offspring phenotypes and offspring segregation ratios can be measured directly in nature. Table 1 shows segregation data for green and chlorophyll-deficient embryos for 27 different mangrove trees. In 26 trees, the ratio of mutant to green embryos is ~3:1, that is, all of the χ^2 values are nonsignificant.

Summing the data in Table 1 (excluding the presumptive chimaera, J) results in a 3.1:1 ratio of green to white embryos. These segregation data are very compelling evidence that the mangrove populations studied were primarily self-pollinated. If outcrossing occurred to any significant degree, the frequency of mutant embryos per tree should be much less than 25%. Thus a mangrove tree and its attached viviparous embryo can be treated as a controlled breeding experiment in which the parents and offspring phenotype are known.

In Table 2, we present data for an extensive red mangrove population growing in Pigeon Creek, a coastal lagoon on San Salvador Island open to the Atlantic Ocean. This population has a calculated mutation rate for albinism of 7.4×10^{-3} mutations per haploid genome per generation. Red mangrove trees heterozygous for albinism have been found in Florida and Puerto